Vapor-liquid phase coexistence and transport properties of two-dimensional oligomers

Tarak K. Patra, Abhiram Hens,[a] and Jayant K. Singh[b]
Department of Chemical Engineering, Indian Institute of Technology Kanpur, Kanpur 208016, India

(Received 6 May 2012; accepted 6 August 2012; published online 23 August 2012)

Grand-canonical transition-matrix Monte Carlo and histogram reweighting techniques are used herein to study the vapor-liquid coexistence properties of two-dimensional (2D) flexible oligomers with varying chain lengths (m = 1–8). The phase diagrams of the various 2D oligomers follow the correspondence state (CS) principle, akin to the behavior observed for bulk oligomers. The 2D critical density is not influenced by the oligomer chain length, which contrasts with the observation for the bulk oligomers. Line tension, calculated using Binder's formalism, in the reduced plot is found to be independent of chain length in contrast to the 3D behavior. The dynamical properties of 2D fluids are evaluated using molecular dynamics simulations, and the velocity and pressure autocorrelation functions are investigated using Green-Kubo (GK) relations to yield the diffusion and viscosity. The viscosity determined from 2D non-equilibrium molecular dynamics simulation is compared with the viscosity estimated from the GK relations. The GK relations prove to be reliable and efficient for the calculation of 2D transport properties. Normal diffusive regions are identified in dense oligomeric fluid systems. The influence of molecular size on the diffusivity and viscosity is found to be diminished at specific CS points for the 2D oligomers considered herein. In contrast, the viscosity and diffusion of the 3D bulk fluid, at a reduced temperature and density, are strongly dependent on the molecular size at the same CS points. Furthermore, the viscosity increases and the diffusion decreases multifold in the 2D system relative to those in the 3D system, at the CS points. © *2012 American Institute of Physics*. [http://dx.doi.org/10.1063/1.4747195]

I. INTRODUCTION

With the realization of nanodevices and nanoscale processes, evaluation of the properties of materials at lower dimensions has become a thrust area of research. Examples of low-dimensional systems include monolayers on solid substrates; fluids confined between two plates separated by a distance on the order of the molecular diameter; lipid molecules at the interface between air and water;[1,2] one-dimensional systems such as fluids confined to the corner of a rectangular box;[3] and single-file arrangement of water molecules inside a nanotube.[4] The dimensionality of a system greatly influences the properties of the fluid, as is evident from various systematic studies concerning the effect of confinement on the thermophysical properties of fluids.[1–10]

In order to understand the properties of low-dimensional systems, as a limiting case of complete confinement, various 2D bulk fluid systems such as square well,[11] Yukawa,[12,13] and Lennard Jones[14–16] have been investigated using the theoretical approach, molecular simulation, density functional theory (DFT), and perturbation theory. The phase equilibria of 2D simple Lennard-Jones (LJ) fluids (i.e., monomers) have been reported in multiple studies.[14,17–22] The shapes of the phase diagrams obtained from various studies on 2D systems are not in agreement, particularly for densities at high temperatures (i.e., near the critical temperature).[23] Smith and Frenkel showed that the critical temperature is very sensitive to the truncation of the LJ potential.[24] Similarly, the line tension values calculated using the Monte Carlo simulation[20] and the DFT (Ref. 21) are found to be in disagreement. Santra *et al.*[25] demonstrated that a large cutoff is required for the convergence of the result in the case of the 2D system. Thus, a stronger correlation is present for the 2D system than for the 3D system. Hence, accurate prediction of the physical properties in 2D systems is more challenging.

In addition to the phase diagram, the dynamical properties of low-dimensional systems are important from the practical and fundamental points of view. The diffusivity and viscosity of 3D systems are widely studied properties that have lately come into focus for confined systems.[26–29] Transport properties in confined systems differ significantly from those in the bulk, since the hydrodynamics and rheology become increasingly complicated as the spatial dimension decreases.[7,30] For example, polymer melts show very strong structural correlation when the confinement is of the order of the polymer size.[2] Overall, confined fluids exhibit high shear viscosity, prolonged relaxation, and nonlinear response at low shear rates as the confinement increases.[31] Thus, autocorrelation functions (ACFs), which describe the correlation of various physical properties as the system evolves in time (in two dimensions), are of great importance. Velocity autocorrelation function (VACF) and stress autocorrelation function (SACF) are two important quantities that are commonly used to understand the dynamical behavior of fluids. ACFs are generally

[a]Present address: Central Mechanical Engineering Research Institute, Durgapur 713209, India.
[b]Author to whom correspondence should be addressed. Electronic mail: jayantks@iitk.ac.in.

calculated using equilibrium molecular dynamics (EMD).[32] Integrations of the VACF and SACF, which are also known as Green-Kubo (GK) relations, provide the self-diffusion coefficient and viscosity of the system, respectively. However, calculation of diffusion and viscosity using ACFs suffers from the problem of convergence. Hence, non-equilibrium methods are being widely used for calculating transport properties. For example, the viscosity of Lennard-Jones chain (LJC) particles in three dimensions in various states has recently been studied by Galliero and Bonded[26] using non-equilibrium molecular dynamics (NEMD). Similarly, the self-diffusion coefficients of 3D LJC fluids at various densities and temperatures have been obtained by determining the slope of the mean square displacement (MSD) curves. MSD is advantageous in that it allows for the detection of diffusive regions, and it is very useful for calculating the self-diffusion coefficient, particularly when the decay of the VACF is not well understood.

In 1970, Alder and Wainwright reported a long-time power law decay ($t^{-d/2}$, where d is the dimension of the system) of the VACF in their pioneering work on moderately dense hard-sphere fluids using MD simulations.[33] This power law leads to a logarithmic divergence of the GK relation in 2D. Until very recently, the use of GK relations to calculate the transport properties in 2D systems was questionable. However, in a recent study, Isobe showed that the 2D VACF of a hard-sphere fluid converges in the long time limit for a moderately dense fluid.[34] Isobe demonstrated that when a large sample population, long correlation time, and more accurate VACF are used, the VACF decays moderately faster than the earlier reported rate of[33] $\sim t^{-1}$. On the other hand, the ACFs of dense systems show oscillatory behavior rather than algebraic decay at a long time.[35] For a dense system, physical processes such as backscattering may occur, which can conceal the non-exponential long-time tail. Hence, capturing the important fluctuation and essential decay of the ACF may involve numerical errors. In a recent study on 3D LJ fluids, Chen *et al.*[36] demonstrated that by using sufficient statistics and by proper analysis of the data, one can obtain very accurate values of viscosity, which agree well with those obtained from non-equilibrium methods. Several other studies[37–39] have also addressed the issues relating to the convergence of the correlation functions. Hong *et al.*[38] suggested that the integration time needs to be long enough to capture the essential decay of the ACF, and at the same time, it should be short enough to avoid the onset of divergence. However, these studies are based on 3D systems. In the case of the 2D system, the behavior of ACFs is completely different and poorly understood. There are a few reports in which the convergence of the SACF in 2D Yukawa systems is also mentioned.[40–42] However, detailed investigation of the convergence of fluid particles with attractive forces, particularly of chain molecules, is not actively pursued.

In this study, we investigate the phase coexistence and transport properties of 2D oligomers or short-chain molecular fluids. Oligomers are ubiquitous in nature, typified by polybutene, paraffins, and esters. Short, single-stranded nucleic acids are also considered as oligomers. In the present study, a comparison between the 2D and 3D liquid-vapor phase transition and transport properties is also presented. The transport properties of 3D short-chain fluids are separately calculated for meaningful comparison. NEMD and EMD studies are also performed herein for comparison of the transport properties evaluated using both methods. The effect of system size on the ACFs and their convergence is also addressed in the current study. The rest of this paper is organized as follows. The model and method are described in Sec. II. In Sec. III, some details of the simulations are provided, and in Sec. IV, the results are presented and discussed. Finally, concluding remarks are presented in Sec. V.

II. MODEL AND METHOD

A well-established model for studying polyatomic fluids is the chain-like-molecular system, wherein spherical segments are connected. The flexibility of the chain has a significant influence on the phase diagram of the system. For example, the critical point differs for 3D flexible chain molecules with different degrees of flexibility.[43] The present study considers fully flexible chain molecules in two dimensions. The model consists of circular beads connected by fixed bonds. Adjacent beads are separated by a distance of unity. All the beads interact through truncated and shifted Lennard-Jones potential of the form:

$$U^{\mathrm{LJ}}(r_{ij}) = 4\varepsilon\left[\left(\frac{\sigma}{r_{ij}}\right)^{12} - \left(\frac{\sigma}{r_{ij}}\right)^{6}\right] - 4\varepsilon\left[\left(\frac{\sigma}{r_c}\right)^{12} - \left(\frac{\sigma}{r_c}\right)^{6}\right]. \quad (1)$$

Here, ε and σ are the characteristic energy and length, respectively. All quantities are reduced with respect to ε, σ, and M (the mass of each bead). The cut-off radius, r_c, is taken as 4σ. Time is reduced as $t^* = t\sqrt{\frac{\varepsilon}{M\sigma^2}}$. The reduced temperature is given as $T^* = k_B T/\varepsilon$. In this study, we consider oligomers that are short polymer chains with m monomers, where m varies from 1 to 8. The asterisk is hereafter dropped from the symbols for convenience.

The grand-canonical transition-matrix Monte Carlo (GC-TMMC) technique[44,45] is used herein to evaluate the phase equilibria of the system. In the GC ensemble, the chemical potential (μ), temperature (T), and volume (V) are kept constant, whereas the particle number (N), pressure (P), and energy (U) fluctuate. At a given coexistence chemical potential, the macrostate probability distribution shows two peaks corresponding to the stable (or metastable) homogeneous phases. However, the coexistence chemical potential of the system is not generally known *a priori* at the specified temperature. Simulations are performed at an assumed chemical potential, μ_0, which pushes the system to the liquid-like state or vapor-like state, depending on its value. Histogram reweighting is utilized to evaluate the chemical potential at which two phases coexist.[46] The multicanonical sampling technique[47] is used to expedite the sampling, which ensures adequate sampling of all microstates with uniform frequency. The detailed methodology is described elsewhere.[9,48]

To evaluate the interfacial tension, GC-TMMC in conjunction with Binder's finite size scaling analysis[49] is

utilized, as demonstrated in our earlier study.[48] The interfacial energy for a finite-size system with a substrate length, L, is determined from the maximum likelihood in the liquid phase ($\Pi_{\max}^{liq}$) and vapor phase ($\Pi_{\max}^{vap}$), and the minimum likelihood in the interface region ($\Pi_{\min}$), as follows:

$$\beta F_L = \frac{1}{2}\left(\ln \Pi_{\max}^{liq} + \ln \Pi_{\max}^{vap}\right) - \ln \Pi_{\min}. \quad (2)$$

The vapor-liquid interfacial free-energy given by Eq. (3) is thermodynamically related to the line tension and varies with the system size according to Binder's formalism:[49]

$$\beta\tau_L = \frac{\beta F_L}{2L} = C_1\frac{1}{L} + C_2\frac{\ln(L)}{L} + \beta\tau, \quad (3)$$

where τ_L is the interfacial tension for a system of box length L, τ is the boundary tension for an infinite system, C_1 and C_2 are constants, and F_L represents the free energy of the vapor-liquid interface for a finite system of size L. The GC-TMMC simulation at any given temperature is repeated for at least three different box lengths (L), and $\frac{\beta F_L}{2L}$ is determined for each L. Equation (3) is then used to determine τ at the given temperature, T.

Using the coexistence data generated from the GC-TMMC simulations, the critical temperature is calculated using the least-squares fit of the following scaling law:

$$\rho^l - \rho^v = C_1\left(1 - \frac{T}{T_c}\right)^{\beta_c}, \quad (4)$$

where ρ^l and ρ^v are the coexistence liquid and vapor densities at temperature T, respectively. C_1 is a fitting parameter. β_c is fixed at 1/8 which is the 2D critical exponent of the Ising model. The critical temperature, T_c, estimated from Eq. (4) is used to calculate the critical density from the least-squares fit to the law of rectilinear diameter:[50]

$$\frac{\rho^l + \rho^v}{2} = \rho_c + C_2(T - T_c), \quad (5)$$

where C_2 is also a fitting parameter. Similarly, the critical pressure is calculated by fitting the following relation:

$$\ln P = A + \frac{B}{T}, \quad (6)$$

where A and B are fitting parameters.

Additionally, the fourth-order Binder's cumulant of the order parameter along the vapor-liquid coexistence line is calculated for different system sizes to determine the critical temperature of the oligomers. Binder's fourth-order cumulant is defined as[51]

$$U_L = 1 - \frac{\langle M^4\rangle_L}{\langle M^2\rangle_L^2}. \quad (7)$$

Here, M is the appropriate order parameter of the system of size L. In the present study, M represents the deviation from the mean density, $M = \rho - \langle\rho\rangle$. $\langle M^4\rangle$ and $\langle M^2\rangle$ are the ensemble average of the fourth and second moments of the of the order parameter, respectively. At the critical temperature, U_L is independent of the system size.[52,53] In this work, to locate the critical temperatures of oligomers, with $m = 2$–8, U_L was calculated for $L = 20$, 25, and 30 at temperatures below and above the predicted T_c from the scaling law. Intersection of $U_L(T)$ curves for different system sizes represents the critical temperature of the system.

Another approach to calculate the critical temperature in the two-dimensional vapor-liquid system is to extrapolate the line tension curve to the temperature where the value of the line tension goes to zero. In this work, aforementioned approach was also used to estimate T_c.

To obtain the transport properties in the liquid states and supercritical states, as suggested by the phase diagrams, MD simulation was performed separately in a canonical ensemble (NVT), where the particle number (N), volume of the system (V), and temperature (T) remain unchanged during the simulation. In order to calculate the different thermophysical properties, all the phase space variables were recorded for a long time.

The diffusivity was calculated from the VACF and the MSD curve, which are mathematically equivalent. The VACF was integrated to obtain the self-diffusion coefficient as

$$D = \frac{1}{d}\int_{t=0}^{t=\infty}\langle v(t)v(0)\rangle dt, \quad (8)$$

where d represents the dimension of the system. This is the GK relation for diffusion.[32] The diffusion coefficient was related to the slope of the MSD of a particle over time:

$$D = \frac{1}{2d}\lim_{t->\infty}\frac{d}{dt}\langle[r_i(t+t_0) - r_i(t_0)]^2\rangle. \quad (9)$$

Similarly, the equilibrium viscosity was calculated using the GK relation for viscosity:

$$\eta = \frac{V}{k_B T}\int_{t=0}^{t=\infty}\langle\sigma_{xy}(t)\sigma_{xy}(0)\rangle dt, \quad (10)$$

where the shear stress was calculated using the relation

$$\sigma_{xy} = \frac{1}{V}\left(\sum_{i=1}^{N} M_i v_{xi} v_{yi} + \sum_{i=1}^{N}\sum_{j=i+1}^{N} dx_{ij} f_{yij}\right). \quad (11)$$

The terms indicated by v represent the velocity of any particle; f_{ij} is the total force exerted by the ith particle due to the jth particle, and V is the volume of the system.

In order to calculate the viscosity using NEMD simulation, the SLLOD equation coupled with the Nose-Hoover thermostat[54] was utilized to generate planar shear flow:

$$\begin{aligned}
\dot{q}_i &= \frac{p_i}{m_i} + q_i.\nabla u,\\
\dot{p}_i &= F_i - p_i.\nabla u - \frac{p_\eta}{Q}p_i,\\
\dot{\eta} &= \frac{p_\eta}{Q},\\
\dot{p}_\eta &= \sum_{i=1}^{N}\frac{p_i^2}{m_i} - dNk_BT.
\end{aligned} \quad (12)$$

Q, the thermostat mass parameter, is written as $dNk_BT\tau_c^2$, where τ_c is a characteristic relaxation time in the system. The

SLLOD algorithm is well established and has been successfully employed to study various systems[55–57] away from equilibrium. In this formalism, the shear viscosity is calculated from $-\langle P_{xy}/\dot{\gamma}\rangle$, where P_{xy} and $\dot{\gamma}$ are the shear pressure and shear rate, respectively.

III. SIMULATION DETAILS

Phase equilibria study in two dimensions was conducted using square boxes of edge lengths $L = 20{,}25,\ 30,\ 35{,}40$. Simulations with different system sizes were performed to obtain the line tension for a given temperature. The statistical error was calculated on the basis of three independent simulations using different random number seeds. The phase diagrams reported in this paper are based on $L = 40$. The 3D phase diagram for the LJC model is taken from Blas *et al.*[58] for comparison between the 2D and 3D systems.

The transport properties were obtained by both EMD and NEMD simulations. EMD and NEMD simulations were performed for 9000 particles using large-scale atomic/molecular massively parallel simulator (LAMMPS).[59] Simulations were performed in the canonical ensemble (NVT). The equations of motions were integrated using the velocity-verlet algorithm by considering the integration time step $\Delta t = 0.001t^*$. The initial configurations were equilibrated for a period of 50 000 unit time, followed by a production run of 50 000 unit time.

In the EMD simulation, a square box with a periodic boundary was used. The temperature was maintained by a Nose-Hoover thermostat with a relaxation constant of 0.5τ. The time series data for velocity and shear pressure were collected during the simulation. Overlapping time segments starting with different time origins were averaged to calculate the VACF ($\langle v(t)\cdot v(0)\rangle$) and SACF ($\langle \sigma_{xy}(t)\ \cdot\ \sigma_{xy}(0)\rangle$). The VACF was averaged over all the particles in the system, and the MSD was averaged over different time origins and particles of the system.

The NEMD simulations were conducted using SLLOD equations [cf. Eq. (12)] for a triclinic box. The SLLOD equations were implemented using a suitable Lees-Edward periodic boundary condition (PBC) (Ref. 60) that incorporates the effect of a moving boundary while calculating the image particle. The SLLOD algorithm in conjunction with the Lee-Edward PBC generates isothermal homogeneous flow in the x-direction, where the velocity gradient is constant in the y-direction. Further details of the SLLOD algorithm can be found elsewhere.[57,61] The simulations were performed for low shear rates ($\dot{\gamma} < 0.7$). The steady state shear-stress, P_{xy}, was calculated using Eq. (10) and was averaged over time.

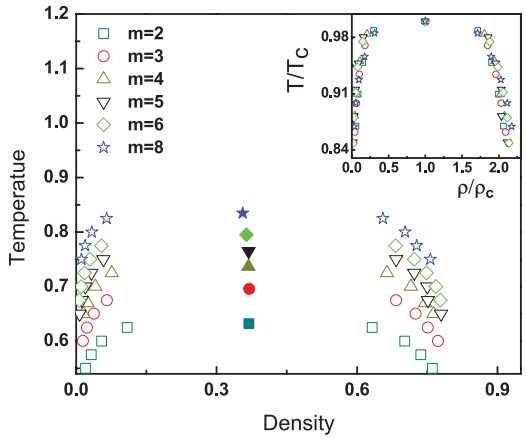

FIG. 1. Temperature-density vapor-liquid coexistence of 2D oligomeric systems. The filled symbols represent the critical points. (Inset) Corresponding state plots of oligomeric systems. Statistical error bars are smaller than the symbol size.

IV. RESULTS AND DISCUSSION

Figure 1 shows the 2D vapor-liquid phase envelope of oligomers with different chain lengths. As expected, the phase envelope shifts to the higher temperature range with increasing chain length. This behavior is well known and has been observed for chain molecules in various studies.[62,63] At a particular temperature, the vapor density of a longer chain is lower than that of a shorter chain, whereas, in the liquid phase, the density of the longer chain is higher than that of a shorter chain. The critical temperatures (T_c), critical densities (ρ_c), and critical pressure (P_c) were calculated by fitting of Eqs. (4)–(6), respectively. Table I summarizes the critical temperatures, densities, and pressures for the chain molecules of different chain lengths considered herein. In addition to the scaling law employed in this work, we also locate the critical temperature where the fourth-order cumulants of different system sizes intersect, as shown in Fig. 2. Table II presents the critical temperature data predicated from both the aforementioned methods. It appears that our estimation of critical temperature by a fit to the scaling law (cf. Eq. (4)) is in good agreement with that predicted from Binder's fourth-order cumulant method. We have further extrapolated the line tension curve to locate the critical temperature where the line tension goes to zero. Table II also lists the critical temperatures obtained from the line tension data. Table II shows that the critical temperature calculated from different methods are in general agreement. Therefore, we conclude that simulation system size considered in this work for the calculation of the critical temperature is sufficiently large and the predicted

TABLE I. The critical temperature, T_c, density, ρ_c, and pressure P_c data of 2D oligomers with variable chain lengths (m). The number in the parentheses represents the error bar in the last digit of the tabled value.

m	2	3	4	5	6	8
T_c	0.630(3)	0.692(1)	0.737(1)	0.765(1)	0.795(2)	0.835(2)
ρ_c	0.3689(5)	0.3693(4)	0.3679(9)	0.368(1)	0.363(3)	0.355(1)
P_c	0.01384(1)	0.00928(4)	0.00675(3)	0.00501(4)	0.00434(9)	0.00367(2)

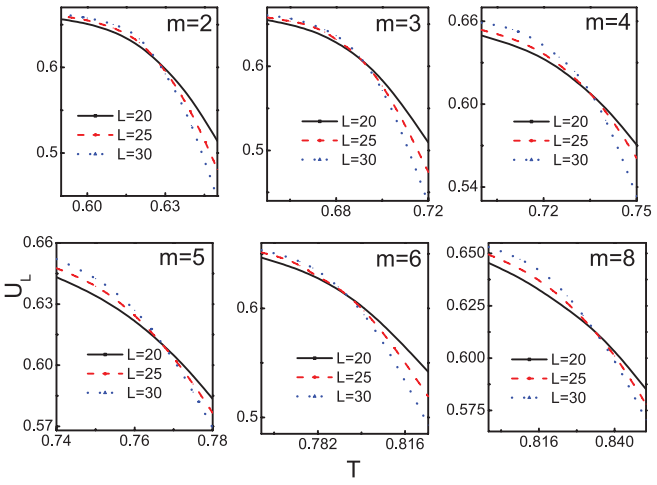

FIG. 2. The fourth-order cumulant, U_L of the order parameter, estimated along vapour-liquid coexistence curve plotted as a function of temperature, T, for different system sizes, L for oligomers with $m = 2 - 8$.

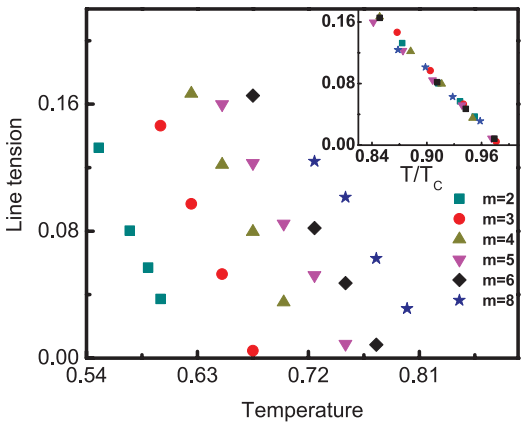

FIG. 3. Vapor-liquid line tension of 2D oligomeric system with variable chain length vs. temperature. Statistical error bars are smaller than the symbol size. (Inset) Plot of line tension versus T/T_c.

critical properties do not associate with the possible system size effects.

It is well known that the critical temperature increases as the length of the polymer chain increases, similar to the behavior observed for the 3D system.[58] The critical temperature is substantially suppressed in the 2D case compared to that in the 3D case, because of the significant reduction in the coordination number. For example, the critical temperature of a tetramer in two dimensions is 0.737 (±0.001) and 2.20 (±0.03) (Ref. 58) in three dimensions. However, this is not the case for the critical density. Our recent work clearly suggests that the critical density can be non-monotonous from 3D to 2D confinement, irrespective of the molecular nature (simple or chain fluids).[64,65] The critical density for a 2D system comprising simple fluids has been observed to be significantly higher than that of the 3D fluid.[9] We observed a similar behavior for the flexible chain molecules. For example, the critical density of tetramer in 3D is 0.265 (±0.005) and 0.367 (±0.009) in 2D. Hence, the critical density in the 2D case is considerably higher than the 3D value. The critical density of bulk 3D flexible chain fluids depends on the size of the chain molecules. In the case of fully flexible bulk (3D) chains, the phase envelopes of short chains ($m = 4 - 8$) become wider with increasing chain length, with a consequent decrease in the critical density.[58] However, in the case of semi-flexible chains for which bond bending and torsion-angle potential must be considered, the critical density increases for short chains (up to eight beads) and decreases for longer chains.[63] In contrast, the critical densities of 2D polymeric fluids do not change significantly with chain length, as shown in Fig. 1. The 2D critical pressure decreases with chain length (cf. Table I); 3D critical pressure data, to the best of our knowledge, are not available for comparison. The inset of Fig. 1 presents the corresponding state (CS) plot of the phase coexistence of oligomers; the temperatures and densities are reduced by the respective critical temperature and critical density of the oligomers in this plot. It is evident from the CS plot that all the phase diagrams fall onto the single curve, indicating that the 2D oligomers conform to the CS principles. This behavior is akin to that observed for the 3D system.[58]

The finite size interfacial energy obtained from five different system sizes using GC-TMMC simulations were extrapolated to obtain the interfacial energy, and consequently the line tension for an infinite system size, as per Binder's formalism.[49] The line tensions of different polymer chains in a 2D environment are shown in Fig. 3 as a function of temperature. The line tension decreased with increasing temperature, as expected, which agrees well with the results of a recent study by Santra and Bagchi[25] on the LJ fluid. The inset of Fig. 3 shows the line tension as a function of reduced temperature. The line tensions of the various oligomers fall on the master curve, which implied that the line tension is insensitive to the chain length for the systems considered herein. Blas *et al.*[58] reported that in the case of the 3D system, the surface tensions of different chain molecules as a function of reduced temperature fall on a single curve when the chain lengths were greater than 8 mer units. Thus, the interfacial tension of 3D oligomers with chain length $m < 8$, at a reduced temperature, depends on the size of the oligomers. On the other hand, the interfacial tension of 2D oligomeric system was found to be independent of the size the molecules.

TABLE II. The critical temperature, T_c of oligomers calculated from different methods. The number in the parentheses represents the deviation in the last decimal point.

m	2	3	4	5	6	8
Binder's cumulant	0.626(1)	0.691(1)	0.734(2)	0.766(2)	0.793(2)	0.834(1)
Extrapolation of the line tension data	0.625(5)	0.688(4)	0.732(6)	0.756(8)	0.781(9)	0.837(7)
Scaling law	0.630(3)	0.692(1)	0.737(1)	0.765(1)	0.795(2)	0.835(2)

Subsequently, the transport properties of 2D oligomers were analyzed, and the VACF and SACF were studied in the liquid and supercritical regions. First, the convergence of the GK relations in two dimensions was investigated, and then, the transport coefficients estimated from the GK relations were compared with those calculated from other methods. The convergence of the SACF is presented in Subsection IV A, and the viscosity calculated from the GK relation is compared with that calculated from the NEMD simulation. The convergence of the VACF is discussed in Subsection IV B, and a comparison is made with the values calculated from the MSD. To facilitate effective comparison of the transport properties of different oligomers, the transport properties were studied at CS points, and for better comparison with the bulk state, the 3D transport coefficients were also calculated at these CS points.

ACFs may be influenced by the "artificial" PBC. To prevent such an effect, it is necessary to choose the maximum correlation time, $t_{\max}(\sim (N/\rho)^{1/3}/c_s)$, which is smaller than the time required for a sound wave to traverse the box. Here, c_s represents the speed of sound, which is calculated as[66]

$$c_s = \sqrt{\frac{1}{M}\left(\frac{\partial P}{\partial \rho}\right)_T + \frac{T}{M\rho^2\left(\frac{\partial E}{\partial T}\right)_S}\left(\frac{\partial P}{\partial T}\right)_S^2}, \qquad (13)$$

where E is the energy per particle, P is the system pressure, and S is the surface of the system. Hence, the box size should be sufficiently large such that $t_{\max}$ is greater than the maximum correlation time being studied. In this study, we investigated the correlation functions up to $t_{\max}$. In Subsections IV A and IV B, a case study is presented for $\rho = 0.7$ and $T = 3.0$; the corresponding $t_{\max}$ values for $m = 1$, 4, and 8 are 8.85, 26.25, and 33.96, respectively.

A. SACF and viscosity

The SACFs were calculated for three chain lengths, viz., $m = 1$, 4, and 8. Figure 4 shows the SACFs at a reduced density of $\rho = 0.7$ and a reduced temperature of $T = 3.0$. The SACFs exhibited oscillatory behavior at a long time in all the cases. This behavior became more prominent with increasing chain length, as shown in Fig. 4. Oscillatory behavior at a long time has also been reported for 3D systems in high-density regions.[35] Here, all the simulations were performed at higher densities where oscillatory behavior at a long time could be observed. The integrated correlation functions showed plateau regions within $t_{\max}$. The viscosity was calculated using Eq. (10), where the SACF was integrated from $t = 0$ to $t = \infty$. However, in all practical cases, time integration of the SACF showed that after a certain initial time, the integration remained unchanged for an ensuing period. The average value of viscosity is generally calculated by averaging the data points from the plateau region of the time integration plot (Fig. 4). The fact that the plateau region can be observed only for a specific time period is in agreement with the observations made in several other studies.[36,38,39] The MD simulations performed herein were based on a sufficiently large system, and the correlation functions were averaged over 10 000 data points. Furthermore, field-driven NEMD simulations were performed for comparison with the viscosity calculated from the GK relation. Figure 5 shows the Newtonian behavior of the system at low shear rates, where the viscosity is independent of the shear rate. NEMD studies at low shear rates ($\dot{\gamma} < 0.7$) did not furnish any evidence of shear thinning. Given that we are comparing the shear viscosity calculated from NEMD simulations with that calculated from the EMD simulation, which essentially represents the case $\dot{\gamma} = 0.0$, we restrict our discussion to the Newtonian regime. Figure 6 shows the viscosity calculated from EMD and NEMD simulations; the viscosity from the NEMD simulation is shown for a shear rate of 0.05. The viscosity data obtained from the GK relation herein was found to be in good agreement with that calculated from NEMD simulations.

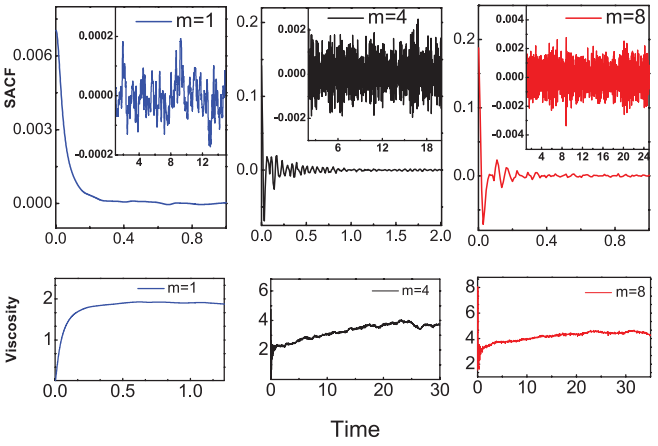

FIG. 4. The SACFs vs. time in reduced unit for m = 1, 4, and 8 are shown in the top images. The long time behavior is shown at the inset of the top images. At bottom, the running time integrations [cf. Eq. (9)] of the SACFs are shown up to the plateau region.

B. VACF and diffusion

Figure 7 shows the MSD curve at a density of $\rho = 0.7$ and temperature of $T = 3.0$. In the diffusive region, MSD $\sim t^{1.0}$ could be clearly observed from the very early stage of the time series. The running derivative of MSD, shown in the inset of the figure to verify the more stringent criteria of

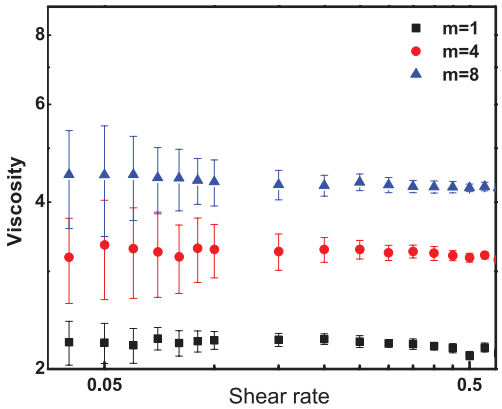

FIG. 5. The shear viscosities calculated from NEMD at different shear rates. Temperature and density are fixed at 0.7 and 3.0, respectively.

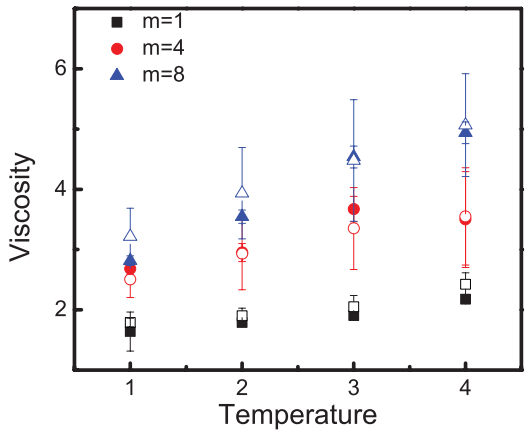

FIG. 6. The viscosities for oligomers calculated from EMD and NEMD at $\rho = 0.7$ for different temperatures. Open symbols correspond to NEMD and closed symbols correspond to EMD.

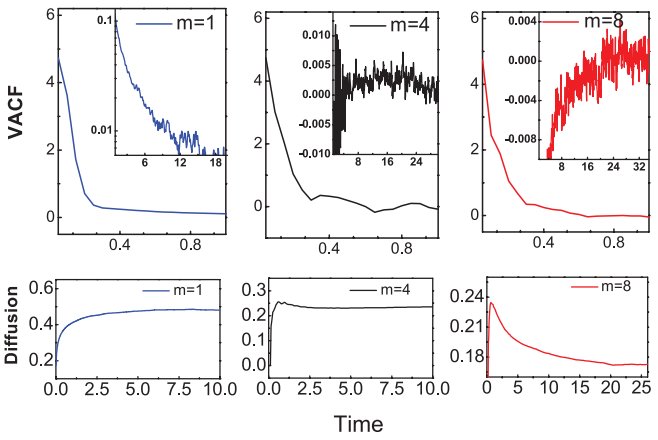

FIG. 8. The VACFs vs. time in reduced unit for m = 1, 4, 8 are shown in the top images. The long time behavior is shown at the inset of the top images. At bottom, the running time integrations [cf. Eq. (7)] of the VACFs are shown up to the plateau region.

diffusion, clearly satisfied the condition $\frac{d}{dt}(\text{MSD}) \sim t^0$. Hence, by performing MD simulation on a moderately large system, we confirmed that a normal diffusive regime exists in dense 2D oligomers. Then, we focused on diffusion coefficient calculation using the GK relation; the VACF and its integration for $m = 1$, 4, and 8 are presented in Fig. 8. Clearly, at a long time, the oscillatory behavior was dominant, as was also observed for SACF. The integrated VACFs were characterized by a plateau region, which could be considered suitable for the diffusion calculation. This plateau region occurred well before $t_{\max}$. The data points within the plateau region were averaged to calculate the diffusion coefficients for all of the systems considered in this study. The estimated diffusion coefficients were in good agreement with the values calculated from the MSD time series. The diffusion coefficients estimated from the MSD [cf. Eq. (9)] and the GK relation [cf. Eq. (8)] at various temperatures using a reduced density of $\rho = 0.7$ are shown in Fig. 9 as an example. The estimated values were in agreement within the error limits.

C. Transport properties at CS points

In this section, we present the transport coefficients at CS points. In order to understand the effect of chain length for different dimensions, we also calculate the transport properties for 3D systems at the selected CS points. Since 2D and 3D both follow the CS principles, CS data point is a convenient state point for comparison. The diffusivities of all of the oligomers at different state points are shown in Fig. 10(a). The diffusivity decreased with increasing polymer size in a nonlinear fashion at all the given temperatures. For a particular oligomer, the diffusivity increased with temperature, because of the high kinetic energy. The nonlinear changes in diffusion with temperature and chain length are reported for 3D systems also.[27] The diffusion coefficients are tabulated in Table III. The diffusion coefficients for chains with $m \geq 5$ did not vary significantly away from the critical temperature. This indicated that the influence of chain length on diffusion diminished for longer chains at the CS points. This behavior was observed both in the liquid region and in the supercritical region. To understand if such a behavior is exhibited in the bulk state, the diffusion coefficients were

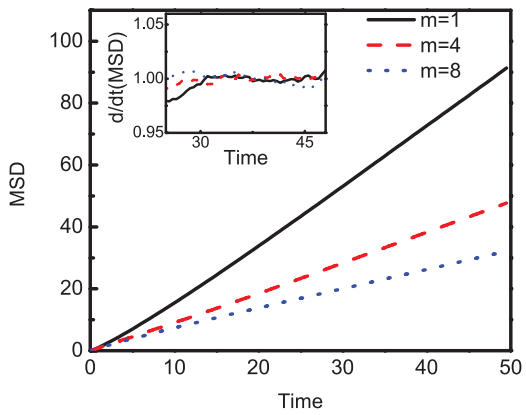

FIG. 7. Mean square displacement (MSD) vs. time for oligomeric systems at $\rho = 0.7$ and $T = 3.0$. Inset shows its time derivative.

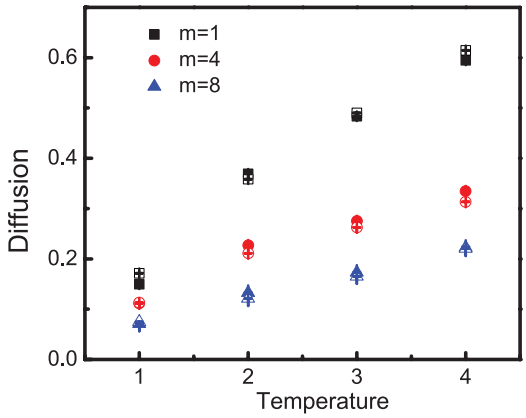

FIG. 9. The diffusion coefficient calculated from VACF [cf. Eq. (7)] and MSD [cf. Eq. (8)] at different temperatures at $\rho = 0.7$. Open symbols correspond to VACF and closed symbols correspond to MSD.

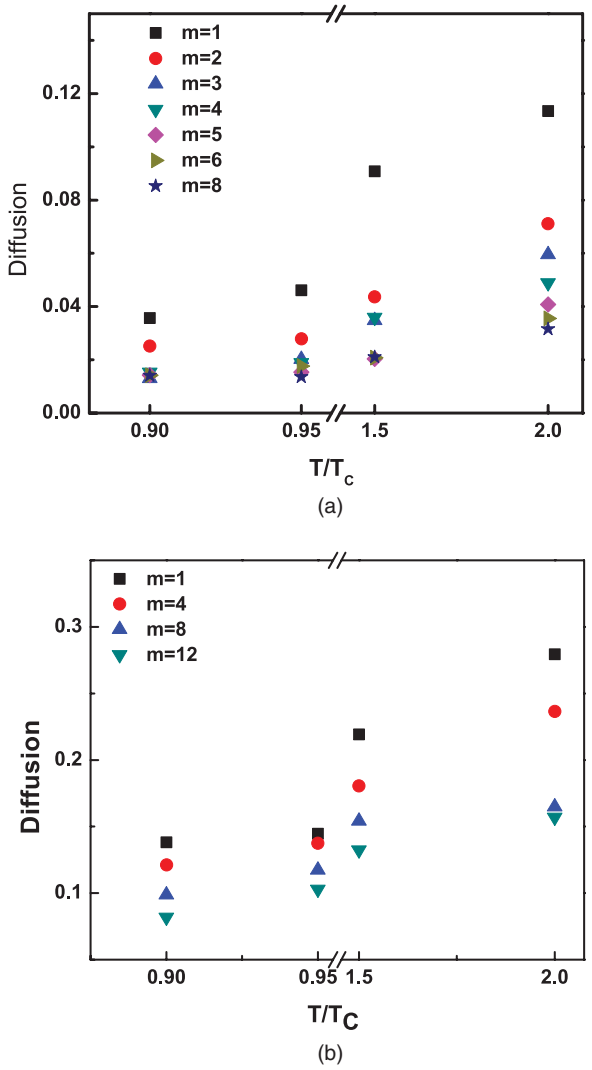

FIG. 10. (a) The 2D diffusion coefficient of oligomers vs. reduced temperature. The reduced density ρ/ρ_c is fixed at 2.25. Error bars are of the order of symbol sizes. (b) The 3D diffusion coefficient of oligomers vs. reduced temperature. The reduced density ρ/ρ_c is fixed at 2.25. Error bars are of the order of symbol sizes.

TABLE III. The 2D and 3D self-diffusion coefficients at $\rho/\rho_c = 2.25$. The number in the parentheses represents the error bar in the last digit of the tabled value.

m	$T/T_c = 0.9$	$T/T_c = 0.95$	$T/T_c = 1.5$	$T/T_c = 2.0$
		2D		
1	0.0357(1)	0.04611(8)	0.0908(2)	0.1134(3)
2	0.02519(6)	0.02787(5)	0.0436(2)	0.0711(4)
3	0.0129(1)	0.0202(2)	0.0348(1)	0.0594(3)
4	0.0153(3)	0.0188(1)	0.0359(3)	0.0489(2)
5	0.01423(9)	0.0153(1)	0.0203(2)	0.0308(2)
6	0.0141(1)	0.0176(2)	0.0227(1)	0.0355(4)
8	0.0141(3)	0.0135(6)	0.0214(4)	0.0315(6)
		3D		
1	0.1382(4)	0.1447(9)	0.2193(7)	0.2795(7)
4	0.1213(2)	0.1375(3)	0.1806(8)	0.2366(2)
8	0.0986(1)	0.1173(3)	0.1542(5)	0.1648(3)
12	0.0818(3)	0.1029(7)	0.1648(3)	0.1571(5)

TABLE IV. The 2D and 3D shear viscosity coefficients at $\rho/\rho_c = 2.25$. The number in the parentheses represents the error bar in the last digit of the tabled value.

m	$T/T_c = 0.9$	$T/T_c = 0.95$	$T/T_c = 1.5$	$T/T_c = 2.0$
		2D		
1	2.88(2)	2.75(1)	2.28(1)	2.21(1)
2	4.7(1)	4.64(9)	3.95(3)	3.74(3)
3	5.25(2)	4.56(3)	4.41(8)	4.73(3)
4	5.71(3)	5.57(3)	5.3(1)	4.64(7)
5	6.87(5)	6.25(8)	5.57(8)	4.52(8)
6	8.7(1)	6.82(7)	5.2(1)	4.4(2)
8	9.2(1)	7.18(4)	5.42(4)	4.44(6)
		3D		
1	1.32(3)	1.28(5)	1.21(4)	1.17(3)
4	1.5(2)	1.47(2)	1.31(7)	1.35(5)
8	1.65(4)	1.52(8)	1.47(2)	1.48(1)
12	1.73(1)	1.69(3)	1.61(8)	1.54(3)

calculated at the same CS points for the bulk oligomers (3D), as shown in Table III and Fig. 10(b). The diffusion coefficients of the bulk fluids were distinctly different for the various chain lengths at a given CS point, except for $m = 8$ and 12 at $T/T_c = 2.0$. It is plausible that the chain-length independent behavior observed in the 2D case may be observed in the 3D case as well at higher T/T_c or at longer chain lengths.

Now we turn our attention to the viscosities of 2D and 3D oligomers. For the sake of comparison, we choose a state point in the corresponding state with $\rho/\rho_c = 2.25$ and $T/T_c = 2.0$. Figure 11(a) presents the plot of shear viscosity versus reduced temperature for different chain lengths; the corresponding values are tabulated in Table IV. The shear viscosity, as expected, increased with the size of the polymer and decreased with temperature. Furthermore, in the 2D supercritical region, the viscosity of long chains, interestingly, did not differ significantly at the reduced temperatures of $T/T_c = 1.5$ and $T/T_c = 2.0$. However, the shear viscosity was influenced by the chain length in the liquid regions where distinct values of shear viscosity were observed for each of the chain lengths. Analogous shear viscosities for the 3D case at the corresponding reduced temperature and density are listed in Table IV and plotted in Fig. 11(b). The 3D shear viscosity was lower than that of the 2D fluid, but the former also varied slightly with chain length at all temperatures. For example, the relative changes in viscosity at low dimensions for $m = 4$ and 8 at $T/T_c = 0.95$ were $\eta_{m=4}/\eta_{m=1} = 1.98 \pm 0.04$ and $\eta_{m=8}/\eta_{m=4} = 1.61 \pm 0.07$. In contrast, the corresponding changes for the 3D system were $\eta_{m=4}/\eta_{m=1} = 1.13 \pm 0.05$ and $\eta_{m=8}/\eta_{m=4} = 1.10 \pm 0.02$ (the suffix represents the chain length). This difference clearly indicated that the rate of viscosity increment is higher in 2D systems than in 3D systems, as the chain length increases.

The insignificant influence of chain length on high-temperature viscosity and low-temperature diffusion is limited only to the oligomers or fully flexible short-chain molecules considered in the present study. It would be of interest to determine whether the longer chain molecules exhibit behavior similar to that observed in this study at a high density; however, that aspect is not covered in this study. We

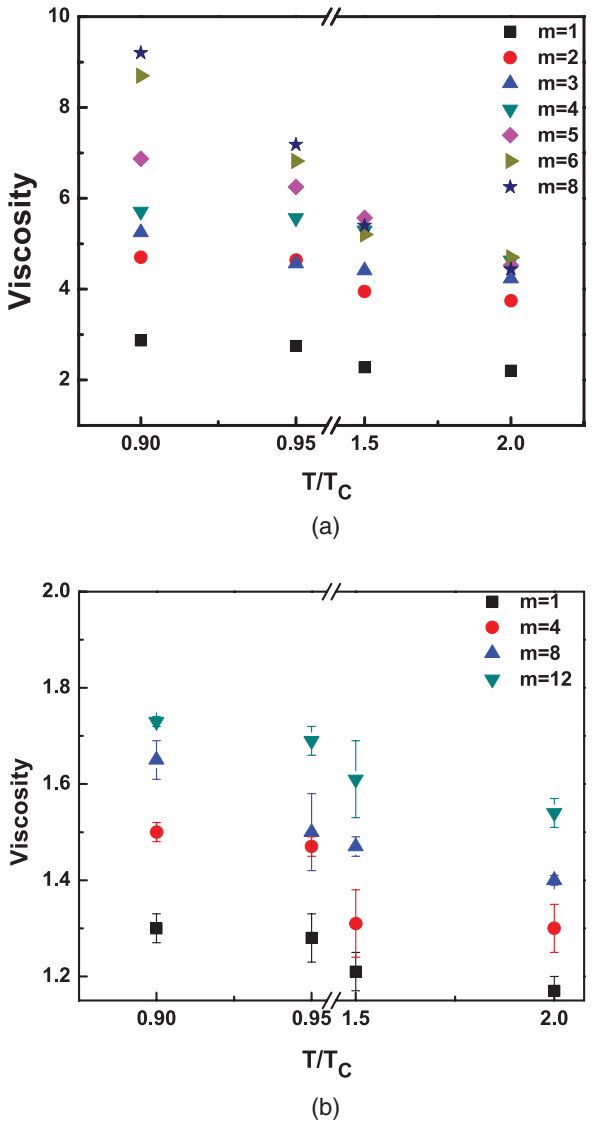

FIG. 11. (a) The 2D shear viscosity of oligomers at different reduced temperatures at a reduced density of $\rho/\rho_c = 2.25$. Error bars are of the order of symbol sizes. (b) Bulk shear viscosities of oligomers vs. reduced temperatures at $\rho/\rho_c = 2.25$.

plan it to investigate the same in the near future. The ratio between the different transport coefficients of the 2D and 3D systems were also calculated at the CS points, as shown in Table V. When the dimensionality was reduced from three to two, the viscosity increased and the diffusion decreased multifold. This change in the transport coefficients was larger for chain molecules than for monomeric fluids. The magnitude of the ratio between the 2D and 3D transport coefficients was also sensitive to the CS points.

TABLE V. The ratio between 2D and 3D transport coefficients of oligomers. The number in the parentheses represents the error bar in the last digit of the tabled value.

m	$T/T_c = 0.9$	$T/T_c = 0.95$	$T/T_c = 1.5$	$T/T_c = 2.0$
		D_{3D}/D_{2D}		
1	3.871(5)	3.138(7)	2.415(5)	2.464(5)
4	7.924(2)	7.313(7)	5.031(1)	4.838(4)
8	6.992(2)	8.682(4)	7.221(2)	5.231(2)
		η_{2D}/η_{3D}		
1	2.18(3)	2.14(4)	1.88(3)	1.63(3)
4	3.81(1)	3.78(2)	4.04(7)	3.43(5)
8	5.57(3)	4.72(5)	3.68(2)	3.01(2)

V. CONCLUSIONS

The thermodynamics and transport properties of oligomers in two dimensions were investigated for various chain lengths ($m = 1 - 8$). GC-TMMC and histogram reweighting techniques were used to determine the phase diagrams of these flexible chain molecules in the 2D system. The phase envelope did not broaden with increasing chain length, contrary to the behavior observed for 3D LJC fluids. Three different methods, viz., scaling law, Binder's fourth-order cumulant approach and extrapolation of the line tension data, were used to evaluate the critical temperature of the oligomers. The values obtained from the methods were in reasonable mutual agreement. Although the critical temperature increased with increasing chain length, the critical density remained almost constant. The phase diagram of short-chain molecules was found to obey the CS principle. Similarly, the line tension for oligomers with $m <= 8$ was found to follow the CS principle in contrast to 3D oligomers. MD simulations were performed to study the dynamical system properties. EMD simulation of 2D oligomers in the liquid and supercritical regions was carried out to calculate the transport coefficients from the fluctuation of the velocity and shear ACFs. Normal diffusion was observed in the dense oligomeric system. GK relations for viscosity and diffusion in the 2D system were found to converge within a suitable time period. Convergence, was however, found to be directly dependent on the chain length. A longer time was required for the convergence of the SACF for the oligomers, as the size of the chain molecules increased. Furthermore, NEMD simulations indicated the existence of a Newtonian regime in the 2D system at low shear rates. The viscosities calculated from EMD and NEMD simulations were in agreement with each other. In the supercritical region, viscosity was not influenced by the size of the molecules. Similarly, in the liquid region, diffusion was not influenced by the size of the oligomers. However, this behavior was not observed for the 3D oligomers. In the case of the 3D system, the diffusion coefficient and shear viscosity varied with the size of the molecules at CS points. A sharp increase in the viscosity and a decrease in the diffusion rate relative to those in the 3D case were also observed for the 2D system. Thus, the results of the current simulation study should prove useful for understanding the general behavior of short-chain oils and biomolecules in a 2D environment.

ACKNOWLEDGMENTS

This work was supported by the Department of Science and Technology, Govt. of India.

[1]V. Prasad, S. A. Koehler, and E. R. Weeks, Phys. Rev. Lett. **97**, 176001 (2006).
[2]A. Cavallo, M. Muller, J. PWittmer, A. Johner, and K. Binder, J. Phys.: Condens. Matter **17**, S1679 (2005).

[3]A. Ghosh, T. K. Patra, R. Kant, R. K. Singh, J. K. Singh, and S. Bhattacharya, App. Phys. Lett. **98**, 164102 (2011).
[4]H. Kumar, B. Mukherjee, S.-T. Lin, C. Dasgupta, A. K. Sood, and P. K. Maiti, J. Chem. Phys. **134**, 124105 (2011).
[5]L. Bureau, Phys. Rev. Lett. **104**, 218302 (2010).
[6]T. Dertinger, I. v. d. Hocht, A. Benda, M. Hof, and J. R. Enderlein, Langmuir **22**, 9339 (2006).
[7]Y. Feng, J. Goree, and B. Liu, Phys. Rev. Lett. **105**, 025002 (2010).
[8]P. Dillmann, G. Maret, and P. Keim, J. Phys.: Condens. Matter **20**, 404216 (2008).
[9]S. K. Singh, A. K. Saha, and J. K. Singh, J. Phys. Chem. B **114**, 4283 (2010).
[10]R. Srivastava, H. Docherty, J. K. Singh, and P. T. Cummings, J. Phys. Chem. C **115**, 10 (2011).
[11]W. Rżysko, A. Patrykiejew, S. Sokołowski, and O. Pizio, J. Chem. Phys. **132**, 164702 (2010).
[12]Y. Feng, B. Liu, and J. Goree, Phys. Rev. E **78**, 026415 (2008).
[13]E. D. Glandt and D. D. Fitts, J Chem. Phys. **66**, 4503 (1977).
[14]J. A. Barker, D. Henderson, and F. F. Abraham, Physica A **106**, 226 (1981).
[15]L. G. V. Goncalves and J. P. Rino, J. Phys.: Condens. Matter **22**, 455106 (2010).
[16]H. Meyer, J. P. Wittmer, T. Kreer, A. Johner, and J. Baschnagel, J. Chem. Phys. **132**, 184904 (2010).
[17]M. Santra, S. Chakrabarty, and B. Bagchia, J. Chem. Phys. **129**, 234704 (2008).
[18]R. R. Singh, K. S. Pitzer, J. J. d. Pablo, and J. M. Prausnitz, J. Chem. Phys. **92**, 5463 (1990).
[19]H. L. Vortler, K. Schafer, and W. R. Smith, J. Phys. Chem. B **112**, 4656 (2008).
[20]J. H. Sikkenka, J. M. J. V. Leeuwena, E. O. Vossnackb, and A. F. Bakkerb, Physica A **146**, 622 (1987).
[21]X. C. Zeng, J. Chem. Phys. **104**, 2699 (1995).
[22]M. Rovere, D. W. Heermanns, and K. Binders, J. Phys.: Condens. Matter **2**, 7009 (1990).
[23]A. Mulero, F. Cuadros, and C. A. Faundez, Aust. J. Phys. **52**, 101 (1999).
[24]B. Smit and D. Frenkel, J. Chem. Phys. **94**, 5663 (1991).
[25]M. Santra and B. Bagchi, J. Chem. Phys. **131**, 084705 (2009).
[26]G. Galliero and C. Boned, Phys. Rev. E **79**, 021201 (2009).
[27]R. A. Reis, F. C. Silva, R. Nobrega, J. V. Oliveira, and F. W. Tavares, Fluid Phase Equilib. **221**, 25 (2004).
[28]D. M. Heyes, J. Chem. Soc., Faraday Trans. **80**, 1363 (1984).
[29]R. Khare, J. J. D. Pablo, and A. Yethiraj, Macromolecules **29**, 9 (1996).
[30]K. J. Strandburg, Rev. Mod. Phys. **60**, 161 (1988).
[31]S. Granick, Science **253**, 6 (1991).
[32]M. P. Allen and D. J. Tildesley, *Computer Simulations of Liquids* (Clarendon, Oxford, 1987).
[33]B. J. Alder and T. E. Wainwright, Phys. Rev. A **1**(1), 18 (1977).
[34]M. Isobe, Phys. Rev. E **77**, 021201 (2008).
[35]A. McDonough, S. P. Russo, and I. K. Snook, Phys. Rev. E **63**, 026109 (2001).
[36]T. Chen, B. Smit, and A. T. Bella, J. Chem. Phys. **131**, 246101 (2009).
[37]Q. Wang, D. J. Keffer, S. Petrovan, and J. B. Thomas, J. Phys. Chem. B **114**, 786 (2010).
[38]B. Hong, F. Escobedo, and A. Z. Panagiotopoulos, J. Chem. Eng. Data **55**(10), 4273 (2010).
[39]M. Mondello and G. S. Grest, J. Chem. Phys. **106**(22), 9327 (1997).
[40]D. Gravina, G. Ciccotti, and B. L. Holian, Phys. Rev. E **52**(6), 6123 (1995).
[41]B. Liu and J. Goree, Phys. Rev. Lett. **94**, 185002 (2005).
[42]Z. Donkó, J. Goree, P. Hartmann, and B. Liu, Phys. Rev. E **79**, 026401 (2009).
[43]C. Vega, C. McBride, and L. G. MacDowell, Phys. Chem. Chem. Phys. **4**, 853 (2002).
[44]J. R. Errington, J. Chem. Phys. **118**, 9915 (2003).
[45]J. R. Errington, Phys. Rev. E **67**, 012102 (2003).
[46]A. M. Ferrenberg and R. H. Swendsen, Phys. Rev. Lett. **61**, 2635 (1988).
[47]B. A. Berg and T. Neuhaus, Phys. Rev. Lett. **68**, 9 (1992).
[48]J. K. Singh and S. K. Kwak, J. Chem. Phys. **126**, 024702 (2007).
[49]K. Binder, Phys. Rev. A **25**, 1699 (1982).
[50]L. J. V. Poolen, C. D. Holcomb, and V. G. Niesen, Fluid Phase Equilib. **129**, 105 (1997).
[51]K. Binder, Phys. Rev. Lett. **47**, 693 (1981).
[52]J. Pérez-Pelliteroa, P. Ungerer, G. Orkoulas, and A. D. Mackie, J. Chem. Phys. **125**, 054515 (2006).
[53]J. Perez-Pellitero, P. Ungerer, and A. D. Mackie, Mol. Simul. **33**, 777 (2007).
[54]M. E. Tuckerman and B. J. Berne, J. Chem. Phys. **97**(3), 1990 (1992).
[55]F. Frascoli and B. D. Todd, J. Chem. Phys. **126**, 044506 (2007).
[56]J. Delhommelle and D. J. Evans, J Chem. Phys. **115**, 43 (2001).
[57]A. Baranyai and P. T. Cummings, J. Chem. Phys. **110**, 42 (1999).
[58]F. J. Blas, L. G. MacDowell, E. d. Miguel, and G. Jackson, J. Chem. Phys. **129**, 144703 (2008).
[59]S. J. Plimpton, J. Comp. Phys. **117**, 1 (1995).
[60]A. W. Lees and S. F. Edwards, J. Phys. C: Solid State Phys. **5**, 1921 (1972).
[61]D. J. Evans, Int. J. Thermophys. **7**, 573 (1986).
[62]J. K. Singh and J. R. Errington, J. Phys. Chem. B **110**(1369), 1369 (2006).
[63]J. Siepmann, S. Karaborni, and B. Smit, Nature (London) **365**, 2 (1993).
[64]S. K. Singh and J. K. Singh, Fluid Phase Equilib. **300**, 182 (2011).
[65]S. K. Singh, A. Sinha, G. Deo, and S. K. Singh, J. Phys. Chem. C **113**, 7170 (2009).
[66]R. F. A. Dib, F. Ould-Kaddour, and D. Levesque, Phys. Rev. E **74**, 011202 (2006).